AGU PUBLICATIONS

Geophysical Research Letters

RESEARCH LETTER
10.1002/2016GL071635

Key Points:
- Full 3-D simulations of the Mars-ionosphere cavity to study Schumann resonances
- Day-night asymmetry on Mars modifies the global Schumann resonance patterns
- Martian dust conditions can modify Schumann resonances, first resonance variations between 9 and 14 Hz

Supporting Information:
- Supporting Information S1
- Figure S1

Correspondence to:
S. Toledo-Redondo,
stoledo@esa.int

Citation:
Toledo-Redondo, S., A. Salinas, J. Portí, O. Witasse, S. Cardnell, J. Fornieles, G. J. Molina-Cuberos, G. Déprez, and F. Montmessin (2017), Schumann resonances at Mars: Effects of the day-night asymmetry and the dust-loaded ionosphere, *Geophys. Res. Lett.*, *44*, 648–656, doi:10.1002/2016GL071635.

Received 18 OCT 2016
Accepted 3 JAN 2017
Accepted article online 6 JAN 2017
Published online 17 JAN 2017

Schumann resonances at Mars: Effects of the day-night asymmetry and the dust-loaded ionosphere

S. Toledo-Redondo[1], A. Salinas[2], J. Portí[3], O. Witasse[4], S. Cardnell[4], J. Fornieles[2], G. J. Molina-Cuberos[5], G. Déprez[6], and F. Montmessin[6]

[1]Science Directorate, European Space Agency, ESA/ESAC, Villanueva de la Cañada, Spain, [2]Department of Electromagnetism and Matter Physics, University of Granada, Granada, Spain, [3]Department of Applied Physics, University of Granada, Granada, Spain, [4]Science Directorate, European Space Agency, ESA/ESTEC, Noordwijk, Netherlands, [5]Department of Electromagnetism and Electronics, University of Murcia, Murcia, Spain, [6]Laboratoire Atmosphères, Milieux, Observations Spatiales (LATMOS), Guyancourt, France

Abstract Schumann resonances are standing waves that oscillate in the electromagnetic cavity formed between the conducting lower ionosphere and the surface of the planet. They have been measured in situ only on Earth and Titan, although they are believed to exist on other planets like Mars. We report numerical simulations of the Martian electromagnetic cavity, accounting for the day-night asymmetry and different dust scenarios. It has been found that the resonances are more energetic on the nightside, the first resonance is expected to be 9–14 Hz depending on the dust activity and to have low quality factors ($Q \simeq 2$). This work serves as an input for the upcoming Exomars surface platform (launch 2020), who will attempt to measure them for the first time.

1. Introduction

Schumann resonances (SR) are standing waves oscillating in the electromagnetic cavity formed by the conducting planetary surface and the lower ionosphere. The first SR mode wavelength is of the size of the planetary circumference. SR are transverse modes to the radial direction (TM_r), with **E** in the radial direction (E_r) and **B** tangential to ground [*Toledo-Redondo et al.*, 2010, Figure 1]. They were predicted by *Schumann* [1952] and first measured on Earth by *Balser and Wagner* [1960]. The main source of energy exciting SR on Earth is lightning and hence their direct link with global climate processes [e.g., *Williams*, 1992; *Price and Rind*, 1994; *Füllekrug and Fraser-Smith*, 1997; *Heckman et al.*, 1998; *Nickolaenko et al.*, 1999; *Williams*, 2005; *Yang and Pasko*, 2007]. Measuring SR on different planets provides valuable information about electromagnetic properties of the cavity, i.e., the composition of its surface, atmosphere, and ionosphere [*Simões et al.*, 2008]. The Huygens descent probe on board the Cassini mission [*Lebreton et al.*, 2005] measured them on Titan [*Béghin et al.*, 2007; *Morente et al.*, 2008; *Béghin et al.*, 2009]. These measurements suggested the existence of a buried ocean in Titan [*Béghin et al.*, 2012]. The main source of excitation of the Titan cavity is believed to be the interaction with Saturn's magnetosphere, which induces large-scale currents on the Titan's ionosphere [*Béghin*, 2014].

Dust storms and dust devils are common on Mars [e.g., *Newman et al.*, 2002; *Ringrose et al.*, 2003], and they have been proposed as a possible source of electric activity [*Farrell and Desch*, 2001; *Kurgansky et al.*, 2007], although no lightning-like signature has been detected so far [*Gurnett et al.*, 2010]. Remote observations using the Deep Space Network found signals that may correspond to SR [*Ruf et al.*, 2009; *Renno and Ruf*, 2012; *Martinez et al.*, 2012]. The ExoMars mission [*Vago et al.*, 2015] included a descent module, expected to land in October 2016, which carried the microAtmospheric Relaxation and Electric field Sensor (μARES) instrument [*Déprez et al.*, 2015], capable of measuring E_r from DC up to 3.2 kHz. After the unsuccessful soft landing of the first ExoMars lander, the second part of the ExoMars mission (to be launched in 2020) will carry another version of an electric field sensor and will constitute the first attempt to characterize the electrical properties of the Martian atmosphere and its global electric circuit, including in situ detection of SR.

Since there are no in situ measurements of plasma properties at altitudes below 80 km on Mars, photochemical models are the best available tool to infer the electromagnetic properties [*Whitten et al.*, 1971; *Molina-Cuberos et al.*, 2001, 2002]. Dust has been found to play a major role in the atmospheric conductivity of Mars by reducing it and enhancing the day-night asymmetry of the Martian cavity, where the conductivity

can differ by 2 orders of magnitude [*Michael et al.*, 2007, 2008; *Aplin*, 2013; *Cardnell et al.*, 2016]. In addition, a layer created by meteoric ablation at 80–90 km of altitude is known to be present [*Molina-Cuberos et al.*, 2003; *Withers et al.*, 2008]. Several works have studied the properties of the SR on Mars [*Sukhorukov*, 1991; *Pechony and Price*, 2004; *Molina-Cuberos et al.*, 2006; *Yang et al.*, 2006; *Soriano et al.*, 2007; *Kozakiewicz et al.*, 2015]. However, the effects of the changing day-night conditions and dust were not considered by these previous studies.

In this work, we model the Martian atmosphere-ionosphere cavity using the Transmission Line Matrix (TLM) method, taking into account the effects of dust and the large day-night asymmetry of the electromagnetic cavity. The effects of the meteoric layer are also investigated. These results serve as a reference for the ExoMars mission in its attempt to measure SR on Mars for the first time.

2. Model

TLM is a time domain numerical method based on discretizing time and space and solves the involved differential equations by approximating the derivatives to differences. Details of the algorithm used can be found in *Toledo-Redondo et al.* [2013, 2016]. The algorithm has been adapted to the size of Mars (radius of 3390 km). We model the spherical cavity formed between the Martian surface and the lower ionosphere, up to 130 km in height, where the conductivity reaches 10^{-3} S/m, and no wave transmission is expected.

First, we validated our model for Mars by computing the resonances for the lossless Martian atmosphere-ionosphere cavity, which has an analytical solution. The first three analytical eigenfrequencies for the ideal Martian cavity are 19.6, 33.9, and 48.5 Hz [*Molina-Cuberos et al.*, 2006]. The estimated eigenfrequencies from our model differ from the analytical solution by less than 3% using a 10 km sampling resolution for each direction and less than 1.5% using a 5 km resolution. We consider the 10 km resolution sufficient for the purpose of this work and for the rest of the study we use this accuracy, with the aim of reducing the computational costs.

The electrical properties of the Martian atmosphere-ionosphere system are obtained from a photochemical model [*Cardnell et al.*, 2016] which uses the Mars Climate Database (MCD) [*Forget et al.*, 1999; *Millour et al.*, 2015] as an input for the properties of the neutral atmosphere. The conductivity profiles used in this work are detailed in Figure S1 in the supporting information and correspond to the conditions expected during the ExoMars landing (October 2016). The major findings that affect SR are the changing conductivity depending on the dust conditions of the atmosphere and the large day-night asymmetry present on Mars. Therefore, we have considered the three dust scenarios defined in *Cardnell et al.* [2016]: low, standard, and high. The standard dust scenario corresponds to a dust distribution reconstructed from seven Martian years (years 24 to 31) of observations, where global dust storms data have been removed. It is referred to as the *climatology scenario* in the MCD. The low dust scenario (*cold scenario* in the MCD) corresponds to an extremely clear atmosphere, i.e., 50% of the dust observed on the clearest day of the seven Martian years monitored. Finally, the high dust scenario (*dust storm scenario* in the MCD) corresponds to the darkest atmosphere to be expected at Mars [*Ockert-Bell et al.*, 1997].

Different methods can be applied to approach the Schumann resonance cavity problem, like, for instance, finite differences in time domain [*Yang et al.*, 2006], 2-D telegraph equations [*Pechony and Price*, 2004], full wave solution [*Galuk et al.*, 2015], or the knee model [*Nickolaenko and Hayakawa*, 2015]. We make use of the 3-D TLM method [*Toledo-Redondo et al.*, 2013, 2016], which can be easily adapted to model the large day-night asymmetry of the Martian cavity. This work considers two kinds of simulations: neglecting the day-night differences (symmetric cavity) and accounting for them (asymmetric cavity). In the former, either day or night conditions are assumed for the whole cavity. This symmetric approach has been widely used in SR studies at Mars [e.g., *Pechony and Price*, 2004; *Molina-Cuberos et al.*, 2006; *Yang et al.*, 2006; *Soriano et al.*, 2007]. We show results from the two approaches for comparison, to illustrate the importance of accounting for the changing day-night conditions in the case of Mars. When the asymmetry is introduced, we assume a sharp (within one step of the grid, 10 km) transition from day to night conditions. Different spatial configurations between the energy source (SR trigger), observation points, and terminator are possible, and we have considered three different cases. Symmetric case with the source at the equator, asymmetric case with the source at the equatorial noon (day-night 1, DN_1) and asymmetric case with the source at equatorial midnight (day-night 2, DN_2). The three cases are detailed in Figures 1–3 (top). The expected fields correspond to B_θ and E_r, the latter being measurable by μARES. The real nature, location, duration, or strength of the electrical sources in the

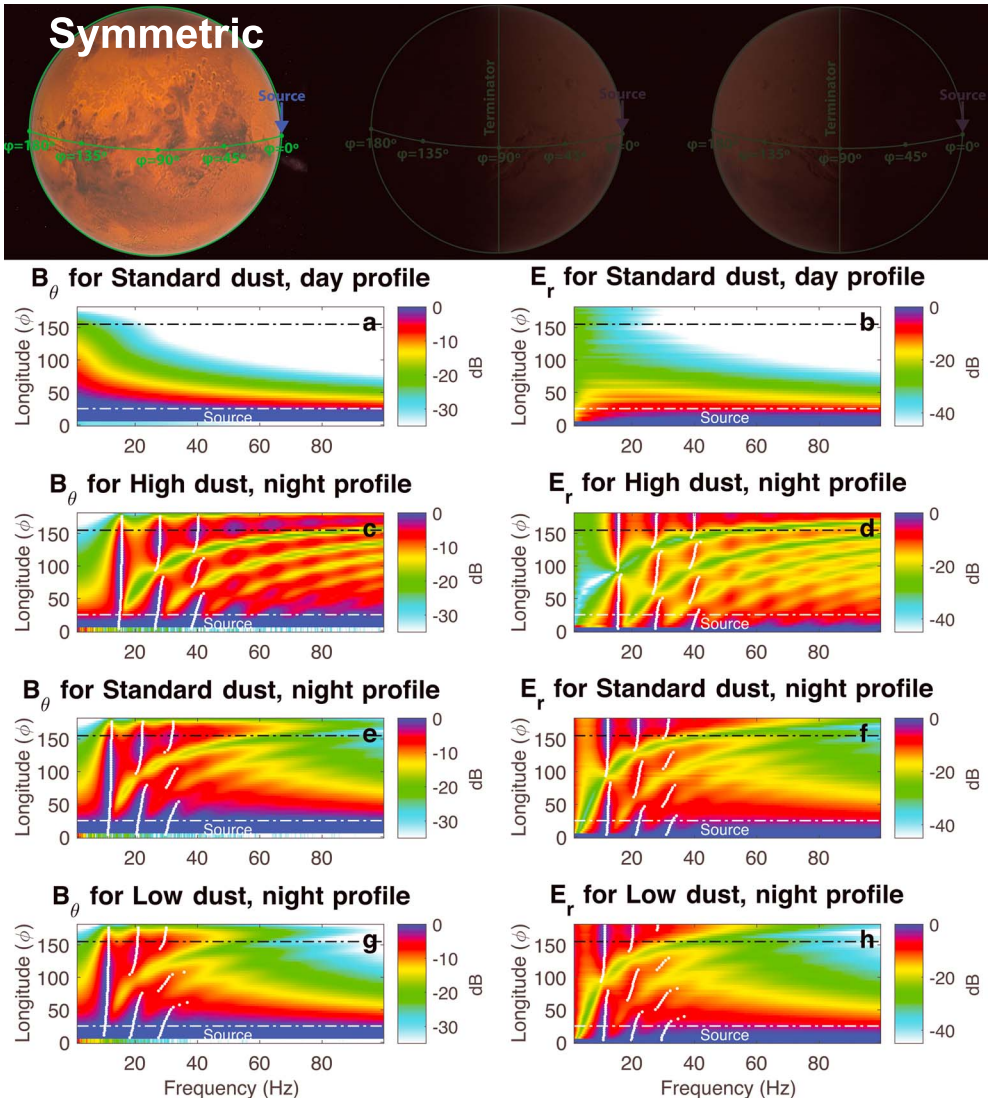

Figure 1. (top) Schematics of the symmetric simulation. (a, c, e, and g) Magnetic and (b, d, f, and h) electric field power spectra as a function of frequency and distance to the source (ϕ), for different conditions of the Martian atmosphere-ionosphere. Figures 1a and 1b correspond to day profile for the standard dust scenario. Figures 1c–1h correspond to night profile for the different dust scenarios (low, standard, and high). The white (black) horizontal dash-dotted lines correspond to cuts at $\phi = 25°$($\phi = 155°$), used in Figure 4.

Martian atmosphere are unknown, although dust storms and dust devils have been proposed as a plausible mechanism. For this study, we used a Gaussian current in the *r* direction, with its energy comprised in the band 0 kHz–1 kHz. The spectrum of this Gaussian current is approximately flat in the SR band. More details on the source used can be found in *Toledo-Redondo et al.* [2016]. We use the same source for all the simulations, i.e., we inject the same amount of energy, and so the SR amplitudes can be compared among simulations. The fields are surveyed along the equator, corresponding to the expected latitude of the landing site of the ExoMars mission (Meridiani Planum, 0.2°N).

3. Results

First, we run our simulation using the symmetric cavity model, i.e., when the day-night asymmetry is not taken into account (Figure 1, top). We use either day or night conditions for the whole cavity and consider different dust scenarios (low, standard, and high). The conductivity profiles for each situation are detailed in the supporting information (Figure S1).

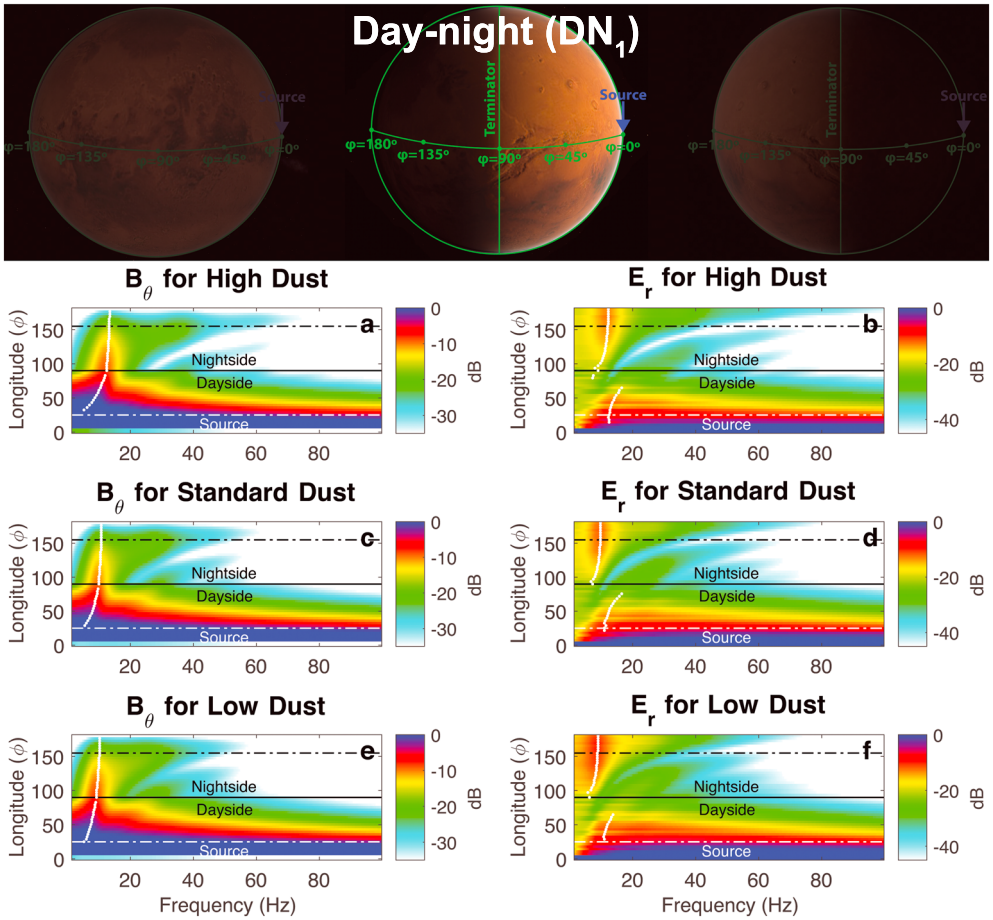

Figure 2. (top) Schematics of the DN_1 simulation. (a, c, and e) Magnetic and (b, d, and f) electric field power spectra as a function of frequency and distance to the source (ϕ), for the different dust scenarios. The white (black) horizontal dash - dot lines correspond to cuts at $\phi = 25°$ ($\phi = 155°$), used in Figure 4.

Figures 1a and 1b correspond to $B_\theta(E_r)$ energy spectrums in the frequency-distance (ϕ) plane for standard dust dayside conditions. The vertical axis (longitude) corresponds to the field surveyed at different distances to the energy source. It can be observed that no SR develop, owing to the large conductivity (losses) of the atmosphere. The wave power is severely damped within one loop around the planet [*Toledo-Redondo et al.*, 2016]. Similar results are obtained when considering low or high dust (not shown). On the other hand, for nighttime conditions, the losses are much lower, and SR are generated (Figures 1c–1h). The lowest atmospheric conductivity occurs for high dust conditions, and therefore, even high modes can be easily identified (Figures 1c and 1d). White dots mark the location of the local maximum for modes 1 to 3, indicating the central frequency of the resonances. The average central frequencies of the modes 1 to 3 are summarized in Table 1, together with their standard deviation (the central frequency changes with the relative distance to the source in a lossy cavity) [*Toledo-Redondo et al.*, 2016]. The first SR is at 11–12 Hz for low and standard dust conditions, but the frequency is shifted up to ~15.5 Hz when high dust conditions prevail. The shift is also observed for f_2 and f_3. High dust conditions decrease the conductivity of the atmosphere, reducing the losses in the cavity, and therefore, the SR are closer to the eigenfrequencies of the lossless cavity.

The results from *Cardnell et al.* [2016] indicate that the Martian atmospheric conductivity varies roughly 2 orders of magnitude at ground level depending on solar illumination. Results from Figure 1 tell us that dayside conditions cannot accommodate SR, while nightside conditions can. The next simulations consider the day and night conductivity profiles on each half of the cavity.

Figure 2 shows the E_r and B_θ components in the frequency-distance plane for the three dust scenarios for the DN_1 case. The results show that only the first mode of the SR develops and is better observed at the nightside, while on the dayside it is difficult to identify the SR, owing to the large damping of the standing

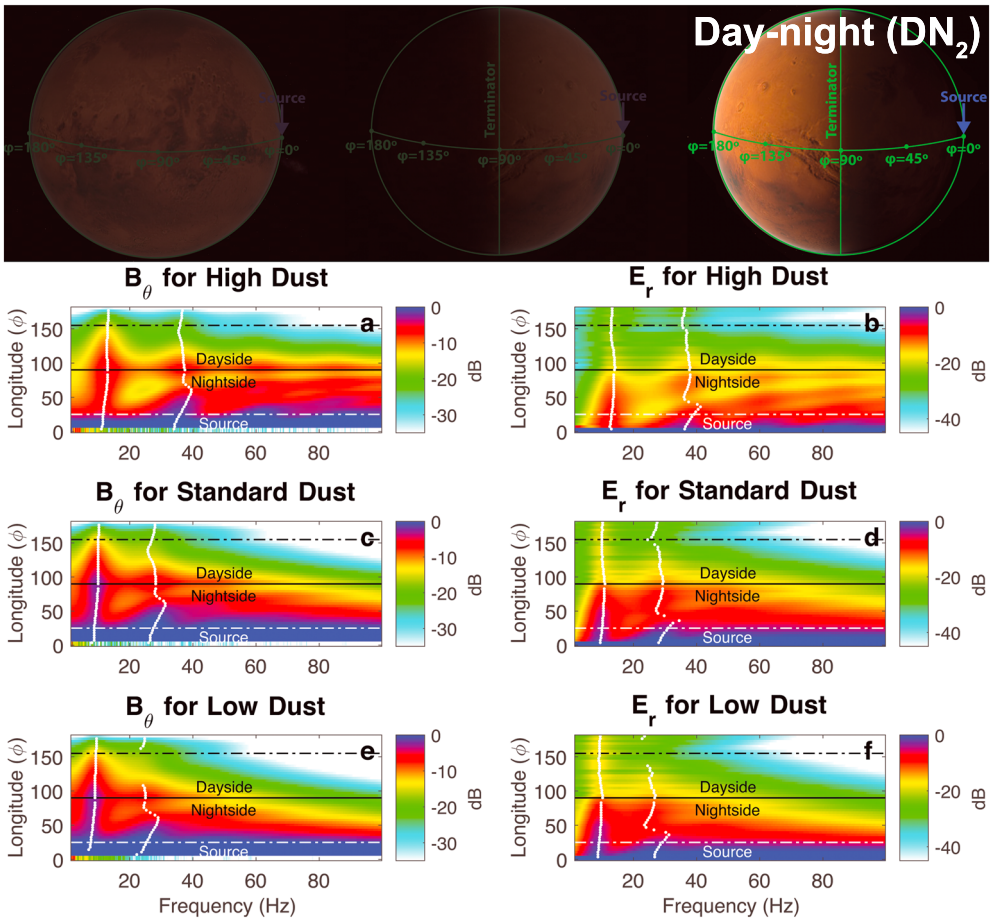

Figure 3. (top) Schematics of the DN_2 simulation. (a, c, and e) Magnetic and (b, d, and f) electric field power spectra as a function of frequency and distance to the source (ϕ), considering the day-night asymmetry of the Martian atmosphere-ionosphere electrical cavity. The white (black) horizontal dash-dotted lines correspond to cuts at $\phi = 25°$ ($\phi = 155°$), used in Figure 4.

Table 1. SR Central Frequencies and Standard Deviation Owing to the Source Distance for the Different Simulations: Symmetric, DN1, and DN2

Simulation		f_1 (Hz)		f_2 (Hz)		f_3 (Hz)	
Profile	Dust	E_r	B_θ	E_r	B_θ	E_r	B_θ
Symmetric	Low	11.2 ± 0.4	11.1 ± 0.5	20.4 ± 1.0	20.2 ± 0.9	30.4 ± 2.2	30.0 ± 2.1
Night	Standard	12.2 ± 0.3	12.1 ± 0.4	22.0 ± 0.7	21.8 ± 0.8	31.4 ± 1.1	31.5 ± 1.1
	High	15.6 ± 0.2	15.5 ± 0.3	27.9 ± 0.6	27.7 ± 0.6	40.0 ± 0.8	39.9 ± 0.9
DN_2	Low	9.4 ± 0.4	8.2 ± 0.6	26.9 ± 2.2	26.1 ± 2.0	-	-
Nightside	Standard	10.3 ± 0.4	9.2 ± 0.5	29.3 ± 1.8	28.6 ± 1.6	-	-
	High	13.4 ± 0.4	12.1 ± 0.6	37.8 ± 1.5	36.9 ± 1.7	-	-
DN_2	Low	9.4 ± 0.4	9.2 ± 0.2	25.4 ± 1.1	24.6 ± 0.5	-	-
Dayside	Standard	10.2 ± 0.3	10.0 ± 0.1	27.8 ± 1.2	27.3 ± 0.9	-	-
	High	13.4 ± 0.4	13.0 ± 0.2	36.7 ± 0.8	36.5 ± 0.6	-	-
DN_1	Low	8.2 ± 0.9	9.8 ± 0.4	-	-	-	-
Nightside	Standard	9.1 ± 0.9	10.5 ± 0.3	-	-	-	-
	High	11.3 ± 1.2	13.0 ± 0.3	-	-	-	-

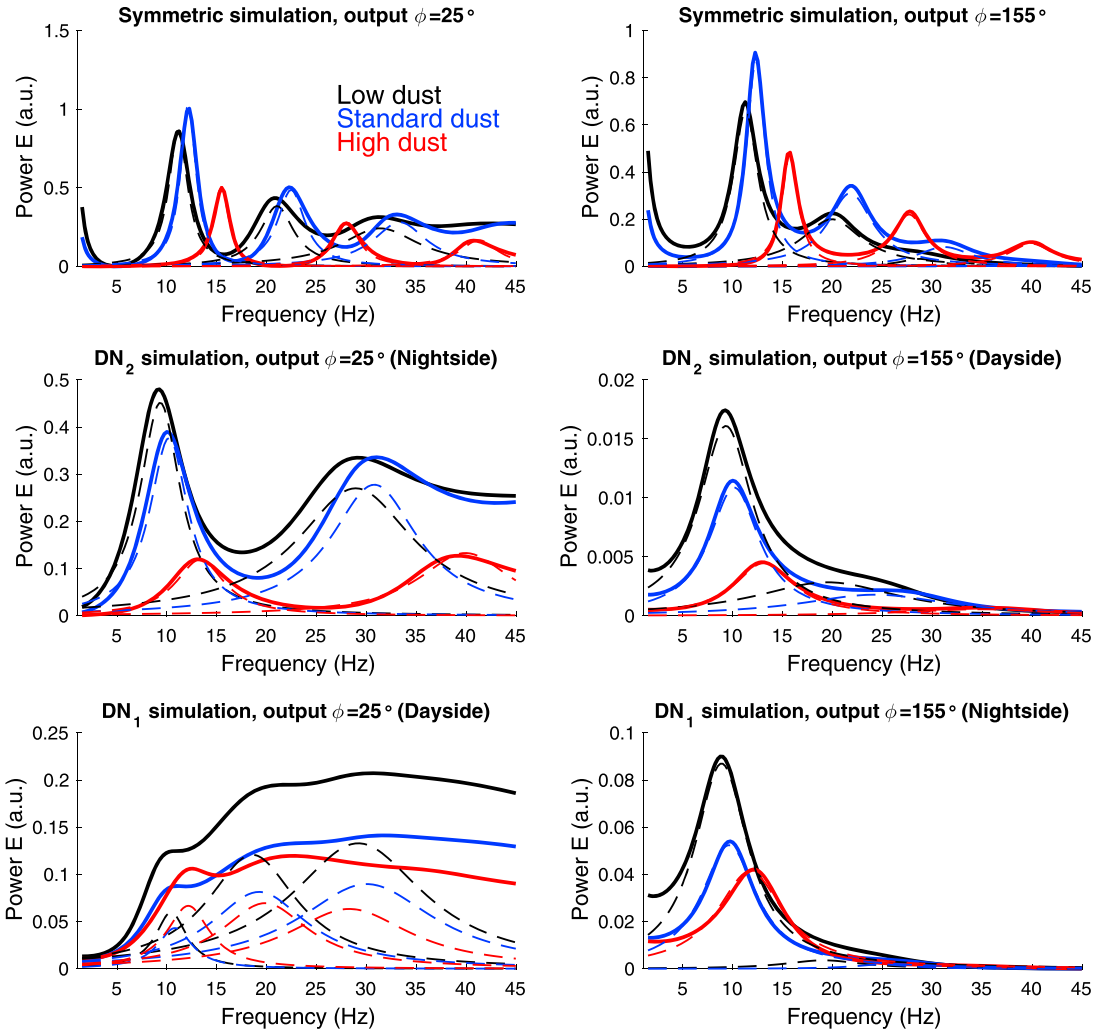

Figure 4. E_r field energy spectrums at (left column) $\phi = 25°$ and (right column) $\phi = 155°$ for three models of the cavity (symmetric nighttime, DN_1, DN_2). Different dust conditions have been considered and are color coded (black, blue, and red). The SR have been fitted by Lorentzian curves, and their parameters are detailed in Table 2.

waves. The central frequencies are significantly different for E_r and B_θ fields and depend on the dust conditions (see Table 1). For the E_r component, the central frequency of the first SR mode changes from 8.2 Hz (low dust) to 11.3 (high dust).

Figure 3 shows the results of the DN_2 case, i.e., day-night asymmetric cavity with the energy source located at midnight. When compared to DN_1, it can be observed that not only the first SR is well defined but also higher modes can be identified, both at the dayside and nightside. The central frequencies of modes 1 and 2, obtained from maximum detection (white dots in Figures 3a–3f), are summarized in Table 1 (DN_2 dayside and nightside). The uncertainties correspond to one standard deviation. The E_r component of the first mode varies between 9.4 Hz (low dust) and 13.4 Hz (high dust) both at the dayside and nightside hemispheres. The B_θ component of the first mode is higher at the dayside than at the nightside. The second mode of the SR is at frequencies significantly larger than for the symmetric case. For instance, for the standard dust scenario, the symmetric-night model predicted 22.0 Hz, while the asymmetric DN_2 model predicts 27.8 Hz and 29.3 Hz at the dayside and nightside hemispheres.

In the previous plots we characterized SR based on the central frequencies of each mode, which were found by detecting maximums of the electric and magnetic energy frequency spectrums. Typically, the nth SR mode is characterized not only by its central frequency (f_n) but also by its maximum amplitude (A_n) and quality factor (Q_n). These parameters are obtained by fitting a Lorentzian curve for each resonance in the energy

Table 2. SR Lorentzian Fit Parameters of E_r: Magnitude (A_n), Central Frequency (f_n), and Quality Factor (Q_n) at $\phi = 25°$ and $\phi = 155°$

			First Resonance			Second Resonance			Third Resonance		
			A_1	f_1	Q_1	A_2	f_2	Q_2	A_3	f_3	Q_3
Night	Low	25°	0.87	11.1	4.9	0.38	21.0	5.2	0.24	31.4	3.3
		155°	0.66	11.3	3.8	0.20	19.9	2.7	0.032	28.7	6.0
	Standard	25°	1.03	12.2	6.5	0.48	22.5	6.8	0.28	33.3	5.0
		155°	0.87	12.3	5.4	0.31	21.8	4.0	0.082	31.2	4.6
	High	25°	0.51	15.5	8.6	0.28	28.1	9.6	0.16	41.3	8.9
		155°	0.48	15.7	7.9	0.22	27.7	6.8	0.10	39.9	7.3
DN_2	Low	25°	0.45	9.3	1.9	0.27	28.9	2.0	–	–	–
		155°	0.02	9.3	1.4	–	–	–	–	–	–
	Standard	25°	0.37	10.2	2.2	0.28	30.8	2.9	–	–	–
		155°	0.01	10.1	1.6	–	–	–	–	–	–
	High	25°	0.12	13.3	2.3	0.13	39.3	3.5	–	–	–
		155°	0.01	13.1	1.8	–	–	–	–	–	–
DN_1	Low	25°	0.06	10.4	2.8	0.12	18.6	1.7	0.13	29.2	1.8
		155°	0.08	8.9	1.5	–	–	–	–	–	–
	Standard	25°	0.04	10.8	2.6	0.08	19.2	1.6	0.09	30.0	1.8
		155°	0.05	9.6	1.4	–	–	–	–	–	–
	High	25°	0.07	12.1	2.3	0.07	19.8	1.9	0.06	28.3	1.9
		155°	0.04	11.7	1.4	–	–	–	–	–	–

spectrum [e.g., *Yang and Pasko*, 2005; *Toledo-Redondo et al.*, 2010]. This fitting is nonlinear and is usually based on iterative processes. We applied Lorentzian fitting to the E_r field energy spectrums marked by horizontal lines in Figures 1–3, corresponding to $\phi = 25°$ (white dotted lines) and $\phi = 155°$ (black dotted lines). For the symmetric case with global dayside conditions (Figures 1a and 1b), SR do not develop, and the Lorentzian fit could not be applied. The rest of the spectrums (symmetric case night conditions, DN_1, and DN_2) and their corresponding Lorentzian fits are plotted in Figure 4. The parameters A_n, f_n, and Q_n for the three first modes ($n = 1, 2, 3$) are summarized in Table 2.

By comparing the A_n SR parameters in Table 2, we can see that the most energetic resonances are produced for the nonrealistic symmetric case, where night conditions were assumed for the whole cavity. For the DN_2 model (energy source at nightside), the SR energy (A_n) is 1 order of magnitude larger at the nightside ($\phi = 25°$) than at the dayside ($\phi = 155°$). On the other hand, for DN_1 the SR energy at dayside and nightside is comparable and much lower than on DN_2 nightside. Therefore, the most favorable scenario to detect SR is when both the detector and the energy source are located at night (DN_2, $\phi = 25°$). Regarding the Q factors, they are smaller than on Earth (losses are higher on Mars). Our estimations for the asymmetric cases are $Q \simeq 2$.

Finally, we run our simulation for the standard dust scenario adding the effect of a layer present at ~85 km, originated by meteoric ablation [*Molina-Cuberos et al.*, 2003], see Figure S1a in the supporting information. We found almost no differences when accounting for that layer.

4. Discussion and Conclusions

The recent findings by *Cardnell et al.* [2016] highlighted the large conductivity differences in the Martian atmosphere depending on solar illumination. Our simulations show that dayside conditions do not allow SR to develop, while nightside conditions, presenting conductivities 2 orders of magnitude lower, do (Figure 1). In addition, the sharp conductivity gradient at the terminator is likely to reflect a portion of the energy of the propagating waves, producing new SR modes in the dayside and nightside coupled cavities. This is consistent with the energy distributions shown in Figure 3. When compared to a simulation without asymmetry and terminator boundary (e.g., Figure 1c compared to Figure 3a), the energy maximums and minimums are distributed in a different way. For instance, Figure 3a does not show a minimum for the second mode

($f_2 = 36.9 \pm 1.7$ Hz) at $\phi = 90°$, but a maximum instead. Our explanation is that a superposition of the second SR mode of the whole cavity and the first mode of the night half cavity (the terminator acts as a boundary of the new cavity) coexist at these frequencies.

Another effect that is observed for the asymmetric model is that the central frequency of the SR modes is different for B_θ and E_r components (Table 1, DN_1, and DN_2 at nightside). This may be related to the relative importance between the superimposed modes (mode $n = 2$ of the whole cavity has approximately the same frequency as mode $n = 1$ of the half cavity), and the fact that the E_r field maximums for each mode are collocated with their respective B_θ minimums.

The largest unknown with respect SR at Mars is the generation mechanism. Lightning is believed to possibly occur in dust storms [*Eden and Vonnegut*, 1973; *Melnik and Parrot*, 1998; *Farrell et al.*, 1999; *Renno et al.*, 2003], and dust devils themselves are electrically active [*Crozier*, 1964; *Farrell and Desch*, 2001; *Kurgansky et al.*, 2007]. The amount of energy that these or other mechanisms can generate in the ELF band inside the Martian atmosphere is not known, as well as their spatial distribution or time patterns (daily, seasonal, etc.). All these aspects constrain the chances to effectively measure SR at Mars.

To summarize, we report numerical simulations of the SR to be expected at Mars, based on the latest modeling efforts of the Martian atmosphere-ionosphere chemical interactions and properties. The day-night asymmetry was never addressed before in SR studies at Mars, and our study highlights its importance for assessing the main SR parameters. In addition, the changing global dust conditions of the Martian planet have the ability to modulate the atmospheric conductivity. Under global dust conditions, the central frequencies and quality factors of the SR significantly increase. Finally, the meteoric layer (~85 km) seems to not affect SR. The best chance to detect SR by ExoMars (E_r measurements) is when the detector is at the nightside and then search for the first ($n = 1$) mode at frequencies varying between 9 and 14 Hz, depending on the global dust conditions of the planet. The Q factor is expected to be low ($Q \simeq 2$), making it easier to distinguish from artificial tones, which typically have large Q factors.

Acknowledgments
This work was supported by the Ministerio de Economía y Competitividad of Spain under the project with reference FIS2013-44975-P, cofinanced with FEDER funds of the European Union. S.T.R. holds an ESA research fellowship and acknowledges support from the ESA science faculty of the European Space Astronomy Centre (ESAC). Owing to the large size of the dataset, scientists interested in it are encouraged to contact the authors directly. The atmospheric properties used in the present study have been taken from the Mars Climate Database http://www-mars.lmd.jussieu.fr/.

References

Aplin, K. (2013), *Electrifying Atmospheres: Charging, Ionisation and Lightning in the Solar System and Beyond*, Springer, Netherlands.
Balser, M., and C. A. Wagner (1960), Observations of Earth-ionosphere cavity resonances, *Nature*, *188*, 638–641.
Béghin, C. (2014), The atypical generation mechanism of Titan's Schumann resonance, *J. Geophys. Res. Planets*, *119*, 520–531, doi:10.1002/2013JE004569.
Béghin, C., et al. (2007), A Schumann-like resonance on Titan driven by Saturn's magnetosphere possibly revealed by the Huygens probe, *Icarus*, *191*(1), 251–266, doi:10.1016/j.icarus.2007.04.005.
Béghin, C., et al. (2009), New insights on Titan's plasma-driven schumann resonance inferred from Huygens and Cassini data, *Planet. Space Sci.*, *57*(14), 1872–1888.
Béghin, C., O. Randriamboarison, M. Hamelin, E. Karkoschka, C. Sotin, R. C. Whitten, J.-J. Berthelier, R. Grard, and F. Simões (2012), Analytic theory of Titan's Schumann resonance: Constraints on ionospheric conductivity and buried water ocean, *Icarus*, *218*(2), 1028–1042, doi:10.1016/j.icarus.2012.02.005.
Cardnell, S., O. Witasse, G. Molina-Cuberos, M. Michael, S. Tripathi, G. Deprez, F. Montmessin, and K. O'Brien (2016), A photochemical model of the dust-loaded ionosphere of Mars, *J. Geophys. Res. Planets*, *121*, 2335–2348, doi:10.1002/2016JE005077.
Crozier, W. (1964), The electric field of a New Mexico dust devil, *J. Geophys. Res.*, *69*(24), 5427–5429.
Déprez, G., et al. (2015), *Micro-ARES, An Electric Field Sensor for Exomars 2016*, vol. 10, European Planetary Science Congress, pp. EPSC2015–508, Nantes, France.
Eden, H. F., and B. Vonnegut (1973), Electrical breakdown caused by dust motion in low-pressure atmospheres: Considerations for Mars, *Science*, *180*(4089), 962–963.
Farrell, W., and M. Desch (2001), Is there a Martian atmospheric electric circuit?, *J. Geophys. Res.*, *106*(E4), 7591–7595.
Farrell, W., M. Kaiser, M. Desch, J. Houser, S. Cummer, D. Wilt, and G. Landis (1999), Detecting electrical activity from Martian dust storms, *J. Geophys. Res.*, *104*(2), 3795–3801.
Forget, F., F. Hourdin, R. Fournier, C. Hourdin, O. Talagrand, M. Collins, S. R. Lewis, P. L. Read, and J.-P. Huot (1999), Improved general circulation models of the Martian atmosphere from the surface to above 80 km, *J. Geophys. Res.*, *104*(E10), 24,155–24,175.
Füllekrug, M., and A. C. Fraser-Smith (1997), Global lightning and climate variability inferred from ELF magnetic field variations, *Geophys. Res. Lett.*, *24*(19), 2411–2414.
Galuk, Yu. P., A. P. Nickolaenko, and M. Hayakawa (2015), Knee model: Comparison between heuristic and rigorous solutions for the Schumann resonance problem, *J. Atmos. Sol. Terr. Phys.*, *135*, 85–91.
Gurnett, D., D. Morgan, L. Granroth, B. Cantor, W. Farrell, and J. Espley (2010), Non-detection of impulsive radio signals from lightning in Martian dust storms using the radar receiver on the Mars Express spacecraft, *Geophys. Res. Lett.*, *37*, L17802, doi:10.1029/2010GL044368.
Heckman, S. J., E. Williams, and B. Boldi (1998), Total global lightning inferred from schumann resonance measurements, *J. Geophys. Res.*, *103*(D24), 31,775–31,779, doi:10.1029/98JD02648.
Kozakiewicz, J., A. Kulak, and J. Mlynarczyk (2015), Analytical modeling of Schumann resonance and ELF propagation parameters on Mars with a multi-layered ground, *Planet. Space Sci.*, *117*, 127–135.
Kurgansky, M. V., L. Baez, and E. M. Ovalle (2007), A simple model of the magnetic emission from a dust devil, *J. Geophys. Res.*, *112*, E11008, doi:10.1029/2007JE002952.
Lebreton, J.-P., et al. (2005), An overview of the descent and landing of the Huygens probe on Titan, *Nature*, *438*(7069), 758–764.

Martinez, S., T. Kuiper, W. Majid, C. Garcia-Miro, L. Tamppari, N. Renno, C. Ruf, and J. Trinh (2012), *Study of Electrical Activity in Martian Dust Storms With the Deep Space Network Antennas*, vol. 1, European Planetary Science Congress, EPSC2012–937 pp., Madrid.
Melnik, O., and M. Parrot (1998), Electrostatic discharge in Martian dust storms, *J. Geophys. Res.*, *103*(A12), 29,107–29,117.
Michael, M., M. Barani, and S. Tripathi (2007), Numerical predictions of aerosol charging and electrical conductivity of the lower atmosphere of Mars, *Geophys. Res. Lett.*, *34*, L04201, doi:10.1029/2006GL028434.
Michael, M., S. Tripathi, and S. Mishra (2008), Dust charging and electrical conductivity in the day and nighttime atmosphere of Mars, *J. Geophys. Res.*, *113*, E07010, doi:10.1029/2007JE003047.
Millour, E., F. Forget, A. Spiga, T. Navarro, J.-B. Madeleine, L. Montabone, A. Pottier, F. Lefèvre, F. Montmessin, and J.-Y. Chaufray (2015), *The Mars Climate Database (MCD Version 5.2)*, vol. 10, European Planetary Science Congress, 438 pp., Nantes, France.
Molina-Cuberos, G., J. Lopez-Moreno, R. Rodrigo, H. Lichtenegger, and K. Schwingenschuh (2001), A model of the Martian ionosphere below 70 km, *Adv. Space Res.*, *27*(11), 1801–1806.
Molina-Cuberos, G., J. Morente, B. Besser, J. Portí, H. Lichtenegger, K. Schwingenschuh, A. Salinas, and J. Margineda (2006), Schumann resonances as a tool to study the lower ionospheric structure of Mars, *Radio Sci.*, *41*, RS1003, doi:10.1029/2004RS003187.
Molina-Cuberos, G. J., H. Lichtenegger, K. Schwingenschuh, J. J. López-Moreno, and R. Rodrigo (2002), Ion-neutral chemistry model of the lower ionosphere of Mars, *J. Geophys. Res.*, *107*, 5027, doi:10.1029/2000JE001447.
Molina-Cuberos, G. J., O. Witasse, J.-P. Lebreton, R. Rodrigo, and J. J. López-Moreno (2003), Meteoric ions in the atmosphere of Mars, *Planet. Space Sci.*, *51*(3), 239–249.
Morente, J. A., J. A. Portí, A. Salinas, and E. A. Navarro (2008), Evidence of electrical activity on Titan drawn from the Schumann resonances sent by Huygens probe, *Icarus*, *195*(2), 802–811, doi:10.1016/j.icarus.2008.02.004.
Newman, C. E., S. R. Lewis, P. L. Read, and F. Forget (2002), Modeling the Martian dust cycle 1. Representations of dust transport processes, *J. Geophys. Res.*, *107*(E12), 5123, doi:10.1029/2002JE001910.
Nickolaenko, A. P., and M. Hayakawa (2015), Spectra and waveforms of ELF transients in the Earth-ionosphere cavity with small losses, *Radio Sci.*, *49*(2), 118–130.
Nickolaenko, A. P., M. Hayakawa, and Y. Hobara (1999), Long-term periodical variations in global lightning activity deduced from the Schumann resonance monitoring, *J. Geophys. Res.*, *104*(D22), 27,585–27,591.
Ockert-Bell, M. E., J. F. Bell, J. B. Pollack, C. P. McKay, and F. Forget (1997), Absorption and scattering properties of the Martian dust in the solar wavelengths, *J. Geophys. Res.*, *102*(E4), 9039–9050.
Pechony, O., and C. Price (2004), Schumann resonance parameters calculated with a partially uniform knee model on Earth, Venus, Mars, and Titan, *Radio Sci.*, *39*, RS5007, doi:10.1029/2004RS003056.
Price, C., and D. Rind (1994), Possible implications of global climate change on global lightning distributions and frequencies, *J. Geophys. Res.*, *99*(D5), 10,823–10,831.
Renno, N. O., and C. S. Ruf (2012), Comments on the search for electrostatic discharges on Mars, *Astrophys. J.*, *761*(2), 88.
Renno, N. O., A.-S. Wong, S. K. Atreya, I. de Pater, and M. Roos-Serote (2003), Electrical discharges and broadband radio emission by Martian dust devils and dust storms, *Geophys. Res. Lett.*, *30*(22), 2140, doi:10.1029/2003GL017879.
Ringrose, T., M. Towner, and J. Zarnecki (2003), Convective vortices on Mars: A reanalysis of Viking lander 2 meteorological data, sols 1–60, *Icarus*, *163*(1), 78–87.
Ruf, C., N. O. Renno, J. F. Kok, E. Bandelier, M. J. Sander, S. Gross, L. Skjerve, and B. Cantor (2009), Emission of non-thermal microwave radiation by a Martian dust storm, *Geophys. Res. Lett.*, *36*, L13202, doi:10.1029/2009GL038715.
Schumann, W. O. (1952), Über die strahlungslosen Eigenschwingungen einer leitenden Kugel, die von einer Luftschicht und einer Ionosphärenhülle umgeben ist, *Z. f. Naturforsch. A*, *7*(2), 149–154.
Simões, F., M. Rycroft, N. Renno, Y. Yair, K. L. Aplin, and Y. Takahashi (2008), Schumann resonances as a means of investigating the electromagnetic environment in the solar system, *Planet. Space Sci.*, *137*(1–4), 455–471, doi:10.1007/s11214-008-9398-0.
Soriano, A., E. Navarro, J. Morente, and J. Portí (2007), A numerical study of the schumann resonances in Mars with the FDTD method, *J. Geophys. Res.*, *112*, A06311, doi:10.1029/2007JA012281.
Sukhorukov, A. (1991), On the schumann resonances on mars, *Planet. Space Sci.*, *39*(12), 1673–1676.
Toledo-Redondo, S., A. Salinas, J. Portí, J. A. Morente, J. Fornieles, A. Méndez, J. Galindo-Zaldívar, A. Pedrera, A. Ruiz-Constán, and F. Anahnah (2010), Study of Schumann resonances based on magnetotelluric records from the western Mediterranean and Antarctica, *J. Geophys. Res.*, *115*, D22114, doi:10.1029/2010JD014316.
Toledo-Redondo, S., A. Salinas, J. A. Morente-Molinera, A. Méndez, J. Fornieles, J. Portí, and J. A. Morente (2013), Parallel 3D-TLM algorithm for simulation of the Earth-ionosphere cavity, *J. Comput. Phys.*, *236*, 367–379, doi:10.1016/j.jcp.2012.10.047.
Toledo-Redondo, S., A. Salinas, J. Fornieles, J. Portí, and H. Lichtenegger (2016), Full 3-D tlm simulations of the Earth-ionosphere cavity: Effect of conductivity on the Schumann resonances, *J. Geophys. Res. Space Physics*, *121*, 5579–5593, doi:10.1002/2015JA022083.
Vago, J., O. Witasse, H. Svedhem, P. Baglioni, A. Haldemann, G. Gianfiglio, T. Blancquaert, D. McCoy, and R. de Groot (2015), ESA ExoMars program: The next step in exploring Mars, *Sol. Syst. Res.*, *49*(7), 518–528.
Whitten, R., I. Poppoff, and J. Sims (1971), The ionosphere of Mars below 80 km altitude—I. Quiescent conditions, *Planet. Space Sci.*, *19*(2), 243–250.
Williams, E. (2005), Lightning and climate: A review, *Atmos. Res.*, *76*(1), 272–287.
Williams, E. R. (1992), The Schumann resonance: A global tropical thermometer, *Science*, *256*(5060), 1184–1187, doi:10.1126/science.256.5060.1184.
Withers, P., M. Mendillo, D. Hinson, and K. Cahoy (2008), Physical characteristics and occurrence rates of meteoric plasma layers detected in the Martian ionosphere by the Mars Global Surveyor radio science experiment, *J. Geophys. Res.*, *113*, A12314, doi:10.1029/2008JA013636.
Yang, H., and V. Pasko (2005), Three-dimensional finite difference time domain modeling of the Earth-ionosphere cavity resonances, *Geophys. Res. Lett.*, *32*, L03114, doi:10.1029/2004GL021343.
Yang, H., and V. P. Pasko (2007), Power variations of Schumann resonances related to El Niño and La Niña phenomena, *Geophys. Res. Lett.*, *34*, L11102, doi:10.1029/2007GL030092.
Yang, H., V. P. Pasko, and Y. Yair (2006), Three-dimensional finite difference time domain modeling of the Schumann resonance parameters on Titan, Venus, and Mars, *Radio Sci.*, *41*, RS2S03, doi:10.1029/2005RS003431.